Received: July 21, 2022. Revised: August 21, 2022.

International Journal of
Intelligent Engineering & Systems

http://www.inass.org/

An Improved DCNN Classification based on a Modified U-Net Segmentation Approach for Ovarian Cancer

Pillai Honey Nagarajan[1]* **Tajunisha Nawabjan[1]**

[1]*Department of Computer Science, Sri Ramakrishna College of Arts and Science for Women, Coimbatore, India*
*Corresponding author's Email: honeyreserach@gmail.com

Abstract: In clinical diagnosis, an effective classification of ovarian carcinoma types is highly essential to avoid the number of deaths worldwide. For this reason, deep convolutional neural network (DCNN) has been designed to classify ovarian carcinoma previously. Then, insufficiency of a dataset was handled by augmenting the training samples using deep semi-supervised generative learning (DSSGL). But, these augmented images directly fed to the DCNN without segmentation causes improper classification of ovarian carcinoma in a significant regions. Also, its computation burden is high. Hence in this article, an enhanced U-Net (EUNet) is proposed as a segmentation module with the DSSGL-DCNN framework for enhancing the accuracy of classifying ovarian carcinoma. This EUNet comprises different units: the inception-residual (IR) unit, the dense-inception (DI) unit, the downsampling unit and the upsampling unit to create the feature-level segmented maps for a given CT scan. But, raising the expansion ratio in the DI unit will provide several variables which make the framework more complex and slower to train. So, the feature-level probability map is also generated which is thresholded to binary and fused with the feature-level segmented maps to create the discriminative segmented sample. In ovarian carcinoma classification, the training CT images are first augmented by the DSSGL method and given to the EUNet. The resultant segmented images from EUNet are fed to the fused structure-based DCNN for categorizing the types of ovarian carcinomas effectively. Finally, the testing outcomes reveal that the DSSGL-EUNet-DCNN attains 91.63 % of accuracy for ovarian carcinoma categorization, whereas existing MLR, GoogleNet, DHL, 2-level DTEL and DSSGL-DCNN achieve 80.24 %, 82.39 %, 85.51 %, 87.76 %, and 88.98 % respectively.

Keywords: Ovarian carcinoma classification, DSSGL-DCNN, Segmentation, U-Net, Dense-inception, Inception-res, Downsampling, Upsampling.

1. Introduction

A tumor is a bacterial illness and is triggered to scatter into several cells by uncontrollable cellular metabolism. It's not only an expression for a particular disease but a substantial number of syndromes. The tumor is not linked to a certain area of the body, but starts as an uncontrollable cell compilation in the body and extends across the body when the malignant cells are recreating and entering the tissue. The second possibility is that some cells are less coordinated unlike normal cells since they do not develop into a properly active cell type. Genetic information is frequently known as the act of storing a functioning protein that can either constitute an enzyme or any functional product using a DNA-coded phenotype [1-3]. The regulation of the frequency of genotypes is a major contribution to the maintenance of cell function. Ovarian carcinoma is the most common type of gynecological cancer among different types of cancer. This represents 2.3 % of the entire fatality rate of tumors [4-6]. It has the highest mortality among gynecological diseases, as most cancers are pretty early hospitalized. Efficient medication is used to help treat metastatic cancer cells and also to improve the patients' survivability after surgery to remove the main ovarian carcinoma cells. However, the prognosis is quite challenging and susceptible to human and learning dissimilarities.

From this viewpoint, an uncontrolled cell

colonoscopy is meticulously planned. Subsequently, anatomical and biological tests are carried out. To alleviate inaccuracies, these tests have been performed in unstable conditions; yet the errors are still in place [7]. Recognizing it earlier is the most efficient way to reduce cancer incidence. A broad range of surgical studies and clinical databases for ovarian cancer are probably featured. Bioinformatics research has examined the need for various anatomical structures and deep learning techniques in advancing diagnostic procedures to support earlier recognition by surgeons [8-10]. The mixture of images created from different methods of image analysis and guidance of advanced tomography innovations increase precision in ovarian carcinoma categorization. Deep neural networks (DNNs) with CT scans notably enable extremely effective medications and also drastically reduce fatality rates and prognostic errors [11]. The major advantage of deep understanding is to select expert experience and possibilities from a huge amount of data. Additionally, CT scans have several benefits including widespread usage, better reliability, less expensive and fast scanning duration.

CT scans are therefore applied for the categorization and prognosis of ovarian carcinomas in current medications. Practically, CNN is widely known for the categorization and prognosis of various kinds of diseases with the help of CT scans including the nervous system, lung, epidermis, and so on [12-14]. On the other hand, there is no appropriate classification framework to detect and treat ovarian carcinoma from CT scans. For this reason, a DCNN framework using AlexNet has been introduced to categorize ovarian carcinoma cells by learning the CT scan database in an automated manner. This framework encompasses 5 convolutional (Conv), 3 max-pooling and 2 reconnect layers. Yet, its accuracy was not highly acceptable.

As a result, DCNN was designed using the mixture of AlexNet, VGG and GoogLeNet structures. In this framework, the merging was conducted at the final softmax layers and the softmax scores of all structures were merged by the weighted sum for acquiring the final ovarian carcinoma category. To reduce overfitting, the DSSGL-DCNN framework was designed [15] with the help of the generative adversarial network (GAN) which solves the overfitting challenge. This GAN was considered as the augmentation scheme to augment the number of training images which were later learned by the mixed structure-based DCNN. This learned framework was further applied to the testing images for categorizing ovarian carcinoma. Conversely, the considered images were directly fed to the DCNN classifier without segmenting its significant regions, which leads to an improper classification and a high computation complexity because it was not able to manage a huge quantity of images.

To solve this problem, a segmentation framework is introduced in the DSSGL-DCNN. The segmentation is done by using the U-Net structure which partitions the region-of-interests (ROIs) from the CT scans to classify ovarian carcinoma. This classic U-Net is a pixel-to-pixel, back-to-back fully convolutional network (FCN) having skip units among evaluation and formulation routes [16]. In contrast, it comprises only a few layers and so it is not sufficiently deep to achieve effective segmentation.

Therefore in this paper, a EUNet is proposed as a segmentation module with the DSSGL-DCNN framework. It produces a feature-level segmented sample and a feature-level probability map for enhancing the accuracy of classifying ovarian carcinoma. In this EUNet structure, the inception and the dense connection units are combined into the classic U-Net for enhancing the efficiency of segmenting the ovarian CT scans. It encompasses the analysis and synthesis routes. These routes have different types of units such as the IR unit, the DI unit, the downsampling unit and the upsampling unit. First, the IR unit is used for increasing the network size by modifying the classic Conv layers. Then, the DI unit is used for segmenting the features in ROIs and creating the network deeper with no extra learning factors. Also, the downsampling is used for decreasing the feature maps dimension to speed up the training process and the upsampling block is applied for resizing the segmented feature maps. But, raising the expansion fraction in the DI unit will provide several variables which make the framework more complex and slower to train. For this purpose, the feature-level probability map is further generated which is thresholded to binary and fused with the segmented feature maps to generate the discriminative segmented mask.

This resultant segmented mask is fed to the fused structure-based DCNN for categorizing the types of ovarian carcinomas effectively. Thus, this DSSGL-EUNet-DCNN framework can increase the accuracy of categorizing ovarian CT scans into many types. The remaining sections of this paper are emphasized as follows: Section 2 discusses different deep learning frameworks to recognize and categorize carcinoma. Section 3 describes the EUNet with the DSSGL-DCNN framework for ovarian carcinoma categorization and section 4

displays its effectiveness. Section 5 concludes the work and recommends the upcoming improvement.

2. Literature survey

The potential of MALDI-imaging was examined [17] in a mixture with linear and nonlinear machine learning schemes to categorize epithelial ovarian carcinoma subclasses from tissue microarray. They utilized linear discriminant analysis (LDA), SVMs with linear and radial basis function (RBF) kernels, neural network and CNN to determine classifiers for epithelial ovarian tumor histotypes depending on the MALDI-imaging-derived proteomic signs.

The diagnostic outcomes of in vivo imaging of patients with ovarian lesions was studied [18] by a co-registered photoacoustic and ultrasound system. First, many ovaries from various patients were imaged in vivo. Then, photoacoustic functional features within an ROI in every ovarian tissue were obtained. Also, a t-test was conducted on all features to choose the important features and the independent predictors were measured by analyzing the similarity between every pair of predictors. Further, a generalized linear model (GLM) and SVM were applied to categorize the ovarian lesions.

The entire-slide histopathology scans and proteomics information from serous ovarian carcinoma patients was assessed [19]. Also, CNN structures such as VGGNet, AlexNet and GoogleNet were applied to mix histopathology and practical omics results, as well as, to estimate the patients' response to platinum-based chemotherapy.

An evolutionary multi-objective optimization based tool (EBST) [20] has been designed to find microRNAs with promising biomarkers in ovarian tumors. At first, the serum microRNA profiles were collected and the fisher discriminant ratio (FDR) filtering was done as pre-processing. Then, the modified multi-objective imperialist competitive algorithm was used to choose the relevant feature subsets by optimizing multiple objective functions. Further, the l_1-SVM classifier has been applied to categorize the chosen features.

An integrated method [21] has been developed to choose the features and categorize the ovarian tumor. First, the features were chosen by the different chromosome choice schemes: relationship coefficient, T-statistics and Kruskal-Wallis trial. Then, the chosen characteristics were adopted using the central force adaptation, lighting addition process adaptation, genetic bee colony optimization and artificial algae optimization. Further, the optimized features were categorized with the different classifiers: LDA, K-Nearest neighbor (KNN), logistic regression (LR), SVM with RBF kernel, and multi-layer perceptron (MLP).

A 2-level deep transfer and ensemble learning (DTEL) scheme was designed [22] using CNN and progressive resizing for automated categorization of epithelial ovarian carcinoma from the whole-slide scans. In level 1, the low-resolution patches were given to the pre-learned VGG19 and the final 1000-class FC unit was substituted by the 5-class FC unit. The softmax was performed to find the categorical distribution related to the 5 subclasses of ovarian carcinoma. In the second level, the initial Conv unit of VGG19 was replaced by 2 randomly initialized Conv units at top of the trained network from level 1 to further improve the efficiency. Then, a matrix was generated to combine the patch-level and slide-level categorization and allocate the label to every patch based on the outcomes of the level 2 classifier. At last, a random forest (RF) classifier was applied to predict the whole-slide image-level labels.

A 2D radiomics method was designed [23] with CT to segregate normal and malignant ovarian neoplasms. First, the data about the patients with surgically-verified normal or malignant ovarian carcinomas were collected and split into 2 sets: training and test sets. The ITK-SNAP software was utilized to delineate the ROIs related to the lesions of the maximum diameters in plain CT image slices. Then, the texture characteristics were captured by the analysis kit (AK) software. The training set was utilized to choose the optimal characteristics based on the maximum-relevance minimum-redundancy (mRMR) conditions and the least absolute shrinkage and selection operator (LASSO). Moreover, a radiomics model using multivariate logistic regression (MLR) was applied for classification.

A deep hybrid learning (DHL) structure was developed [24] to categorize ovarian carcinoma. First, the ovarian carcinoma images were preprocessed and given to the 21-layered CNN for feature extraction. This CNN has a series of incept layers and squeeze layers. The extracted features were then classified by the random forest and XGBoost to identify ovarian carcinoma.

2.1 Research contribution

From this survey, it is addressed that the most standard machine learning algorithms are only suitable for segmenting and classifying a small number of training images.

The classification efficiency was reduced [17] since the tiny normal areas may be present in the carcinoma areas. The efficiency was less [18], since the overall number of accessible independent

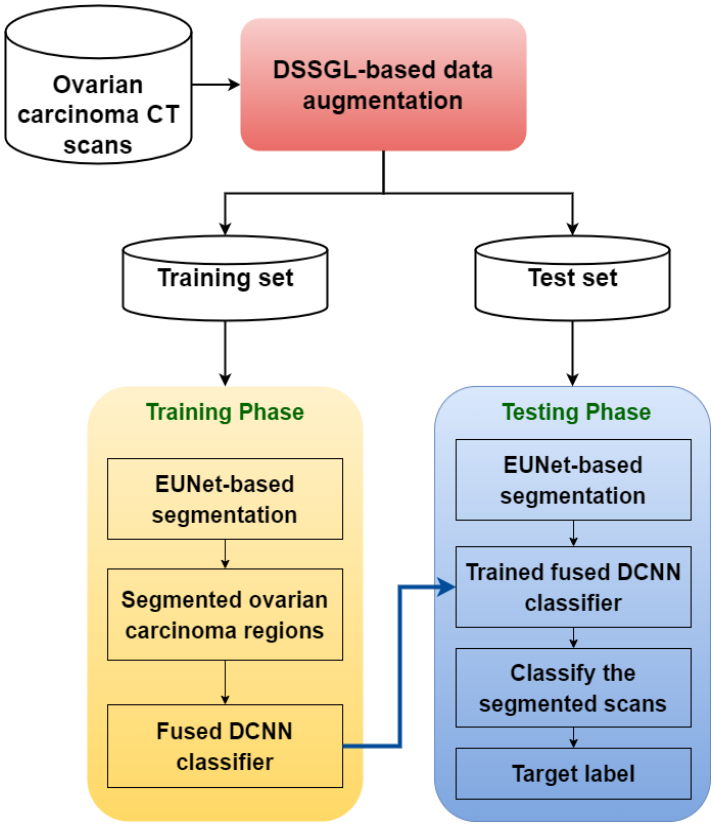

Figure. 1 Schematic representation of DSSGL-EUNet-DCNN framework for ovarian carcinoma categorization

samples was not sufficient for training and testing these classifiers.

Only on serous ovarian carcinoma was focused, whereas other categories of ovarian carcinoma were not involved [19]. An appropriate kernel functions of SVM to be selected [20] properly to achieve better efficiency. The classifiers proposed in [21] have less accuracy and high training time for large-scale datasets.

The accuracy of [22] was not effective since it needs a larger database and segmentation models that involve features from various patch dimensions.

The ROI partition for ovarian carcinoma was conducted manually [23], which provides inter- and intra-observer variability. The analysis [24] was limited to inadequate images and the CNN must be fine-tuned to increase the efficiency.

So, to solve these challenges, this study aims to develop a new model to segment the ovarian carcinoma regions and classify their classes precisely from a large amount of CT images.

3. Proposed methodology

In this section, the DSSGL-EUNet-DCNN-based ovarian carcinoma categorization framework is described in detail and its schematic diagram is portrayed in Fig. 1. First, the training CT images are gathered and the DSSGL is applied as an image augmentation scheme which augments the number of training images. Then, the augmented training samples are given to the EUNet for segmenting ROIs in ovarian CT scans. Further, the segmented feature map is fed to the fused architecture-based DCNN for categorizing ovarian carcinoma. The entire process of this DSSGL-EUNet-DCNN framework is presented in Algorithm 1.

3.1 Image acquisition and augmentation

Initially, the ovarian carcinoma CT scans are collected from the cancer genome atlas-ovarian (TCGA-OV) dataset [25] which encloses the 43 ovarian carcinoma CT scans in DICOM format. These CT scans are augmented by the DSSGL method [15], which uses the semi-supervised GAN model for increasing the number of training samples.

So, it produces a total of 497 images for 7 different ovarian carcinoma classes such as ovarian epithelial tumor, germ cell cancer, sex cord-stromal cancer, serous carcinoma, mucinous carcinoma, endometrioid carcinoma and clear cell carcinoma. Then, those augmented samples are provided to the EUNet for the segmentation process.

3.2 EUNet-based segmentation

The structure of EUNet is illustrated in Fig. 2

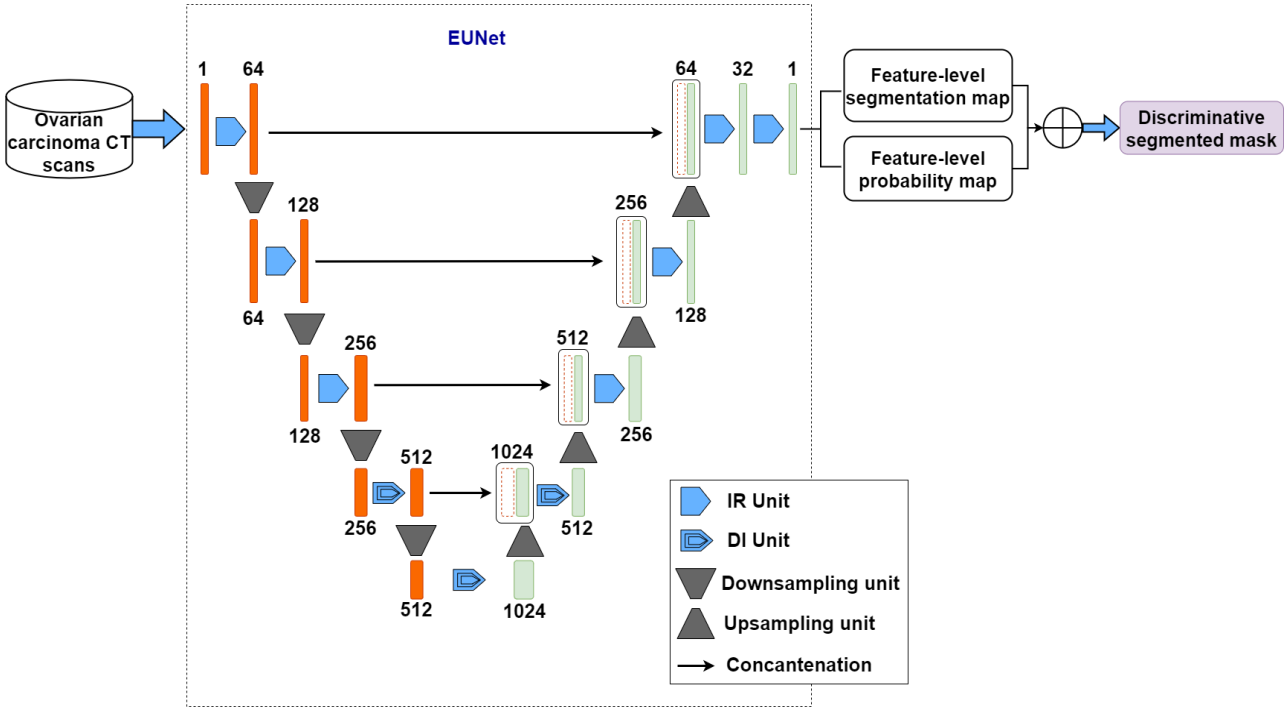

Figure. 2 Overall structure of EUNet for segmentation process

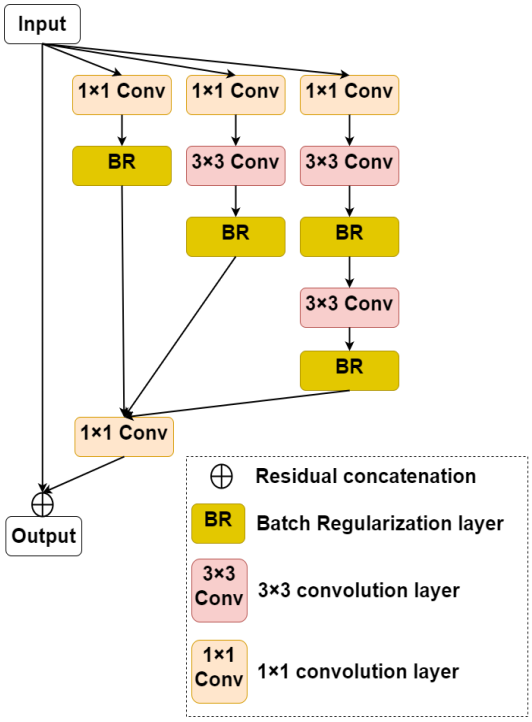

Figure. 3 Overall structure of IR unit

which comprises the analysis route and the synthesis route. Such routes involve 4 different units: the IR unit, the DI unit, the downsampling and the upsampling units. The evaluation route has 3 IR units, 1 DI unit and 4 downsampling units. Similarly, the formulation route has 3 IR units, 1 DI unit and 4 upsampling units. In the mid of the U-Net, 1 DI unit is employed and it has many inception layers compared to others.

3.2.1. IR unit

An adapted residual inception unit is introduced to be utilized in the evaluation and formulation routes. The major aim is to combine attribute maps from various divisions of distinct kernels that will create a system broader and able to train many features. Also, the residual links provide the training simpler because it trains an operation regarding the entry attribute maps rather than training an unreferenced operation. As portrayed in Fig. 3, in this unit, every Conv layer is following the Batch Regularization (BR) excluding bottleneck layers to prevent gradient vanishing when preserving Conv layers.

Consider a_i is the outcome of i^{th} layer, $h_{n\times n}(\cdot)$ is a $n \times n$ kernel Conv layer and $h_r(\cdot)$ is the BR. The operation of concatenation is substituted using the symbol of $\circ$ and 1×1 dimension Conv kernel denotes the bottleneck layer. So, the outcome of the unit from the evaluation route is as:

$$h_{i+1} = h_{1\times1}\left(h_{1\times1}(a_i) \circ h_r\left(h_{3\times3}(h_{1\times1}(a_i))\right)\right) \circ h_r\left(h_{3\times3}\left(h_r\left(h_{3\times3}(h_{1\times1}(a_i))\right)\right)\right) + a_i \quad (1)$$

3.2.2. DI unit

In this unit, the inception unit presented is added into the dense link unit. Via configuring the padding as a matching approach in the Conv layer, the

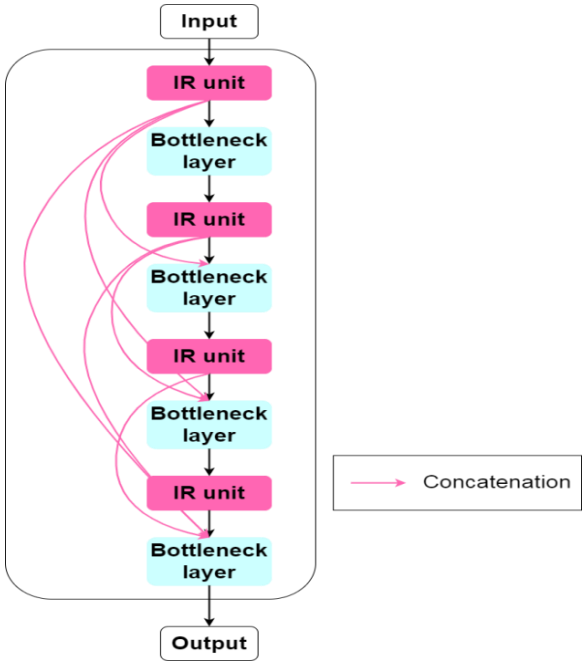

Figure. 4 Overall structure of DI unit

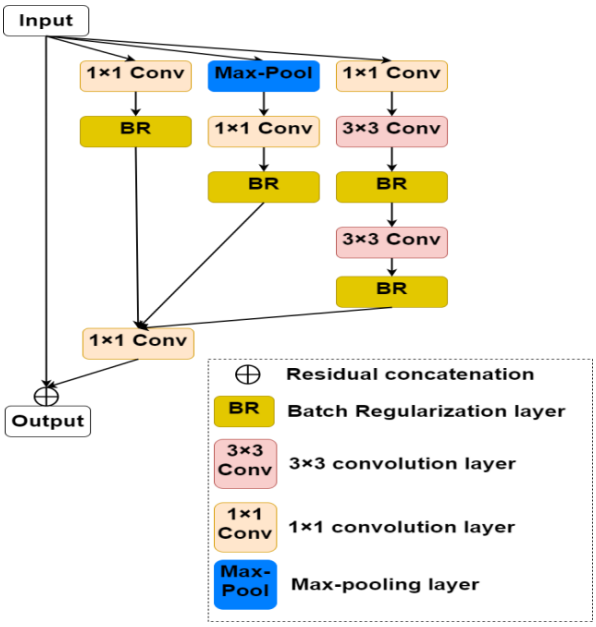

Figure. 5 Overall structure of every IR unit in DI unit

outcomes of the inception unit can stay in the identical dimension of the attribute map as the entries. So, the inception unit is observed as a broader Conv layer because it is a concatenate of various kernel dimensions with pooling layers. The primary goal is to integrate the inception unit into the dense link structure and broader with no gradient vanishing or unwanted estimation.

Fig. 4 depicts the structure of DI unit and Fig. 5 portrays the detail of every IR unit in the DI unit.

The inception unit with the residual link in the dense link unit is varied from the classic IR unit since the BR is employed following every Conv layer. The dense link's major aim is to create the system deeper through concatenating previous Conv outcomes; however narrower with the diminutive hyper-parameter of expansion ratio. So, the dense link unit is fine-tuned for enhancing its efficiency in the dense link unit. Based on this manner, the DI units have been employed in the mid of the U-Net in which the dimension of the attribute map is tiny and a huge kernel is substituted using 2 minor kernels for decreasing the processing difficulty.

Consider $h_{n\times n}(\cdot)$ is a $n \times n$ kernel Conv layer, $h_r(\cdot)$ is the BR and $m_{n\times n}(\cdot)$ is the max-pooling. The symbol $\circ$ denotes the concatenation and $f_{IR}(\cdot)$ is the operation of the bottleneck layer after the new IR unit. So, the outcome of this IR unit is as:

$$a_{i+1} = h_{1\times1}\left(h_{1\times1}(a_i) \circ h_r\left(h_{1\times1}(m_{3\times3}(a_i))\right)\right) \circ h_r\left(h_{3\times1}\left(h_r\left(h_{1\times3}(h_{1\times1}(a_i))\right)\right)\right) + a_i \quad (2)$$

The outcome of $i + 1^{th}$ layer in the DI unit is as:

$$a_{i+1} = f_{IR}([a_0, a_1, \dots, a_i]) \quad (3)$$

In Eq. (3), $[a_0, a_1, \dots, a_i]$ is the concatenation of the attribute maps generated in the layers $0,1, \dots, i$. In total, 3 DI units have been developed: 1 unit is employed in the evaluation route, 1 is in the formulation route and the final unit is applied in the mid of the U-Net. Every DI unit excluding the mid-unit comprises 12 new IR units and the mid-unit comprises 24 IR units. The expansion ratio is considered as the entry of the IR unit. Because of the concatenation link, the dimension of the attribute map is not altered.

3.2.3. Downsampling and upsampling units

These 2 blocks comprise a similar structure excluding the Conv and max-pooling layers in the downsampling unit and the deconvolution and up-sample layers in the upsampling unit. These are observed as a shortened inception unit with 3 divisions. Max-pooling and upsampling 2D layers are applied for decreasing and extending the dimension of feature maps, accordingly which results in feature loss and less precision. So, these issues are solved by these 2 blocks.

Consider $h^2_{n\times n}(\cdot), g^2_{n\times n}(\cdot), m^2_{3\times3}(\cdot)$and $u^2(\cdot)$ are the Conv, Conv transposed, max-pooling and the upsampling with 2 strides. The representation for the downsampling unit is as:

$$a_{i+1} = h_{1\times1}\left(h^2_{3\times3}\left(h_{1\times1}(a_i)\right) \circ h^2_{3\times3}\left(h_{3\times3}\left(h_{1\times1}(a_i)\right)\right) \circ m^2_{3\times3}(a_i)\right) \quad (4)$$

Also, the representation for the upsampling unit is as:

$$a_{i+1} = h_{1\times1}\left(h^2_{3\times3}\left(h_{1\times1}(a_i)\right) \circ h^2_{3\times3}\left(h_{3\times3}\left(h_{1\times1}(a_i)\right)\right) \circ u^2(a_i)\right) \quad (5)$$

The entire network structure is developed followed by the idea of encoder-decoder design with skip links. The encoding task relates to the evaluation route and the decoding task relates to the formulation route. In the encoder, while the learning samples are fed to the network as the entries, the layer index is increased by twice once every IR or DI unit and the dimension of attribute maps is decreased by ½ following the downsampling unit. In the decoder, the layer of attribute maps is decreased by ½ once for every IR or DI unit and the dimension of attribute maps are increased by twice following the upsampling unit. Thus, it segments the ROIs from the CT scans and produces feature-level segmented maps.

To enhance the accuracy, a feature-level probability map is also created which has the highest range of the possibility of each sample being in one of the seven ovarian carcinomas. This map is thresholded to binary and fused with the feature-level segmented maps for generating the discriminative segmented feature map. Consider, the encoder in EUNet creates a L-dimensional feature map y of real values where L is the number of ovarian carcinoma classes. The real values in y are regularized by the softmax factor φ for creating another L-dimensional feature map $\bar{y} = \varphi(y)$. It is appropriate to consider that feature maps with low possibility can have less discriminativeness. If $\max(\bar{y}) > \varepsilon$, then the feature map is termed as discriminative where ε denotes the threshold value.

3.3 Fused DCNN-based classification

After segmenting the training samples, the DCNN classification is performed to categorize ovarian carcinoma. This DCNN is based on the mixture of AlexNet, GoogLeNet and VGG structures [15] wherein the results of each structure are concatenated at the final softmax layer using a weighted sum-rule strategy. This gives the resultant class of ovarian carcinomas precisely. Table 1 lists all the parameters used in this study.

Table 1. Parameters used for DSSGL-EUNet-DCNN

Parameters	Description
a_i	Output of i^{th} layer in IR unit
$h_{n\times n}(\cdot)$	$n \times n$ kernel Conv layer
$h_r(\cdot)$	Batch normalization
$m_{n\times n}(\cdot)$	Max-pooling
$\circ$	Concatenation
$f_{IR}(\cdot)$	Operation of the bottleneck layer after the new IR unit
$[a_0, a_1, \ldots, a_i]$	Concatenation of the attribute maps generated in the layers $0,1, \ldots, i$
$h^2_{n\times n}(\cdot)$	Conv with 2 strides
$g^2_{n\times n}(\cdot)$	Conv transposed with 2 strides
$m^2_{3\times3}(\cdot)$	Max-pooling with 2 strides
$u^2(\cdot)$	Upsampling with 2 strides
L	Number of ovarian carcinoma classes
$\bar{y}$	L-dimensional feature map
φ	Softmax function

Algorithm 1: DSSGL-EUNet-DCNN

Input: Ovarian carcinoma CT scans

Output: Classified categories of ovarian carcinoma

Begin

Acquire the TCGA-OV dataset;

Split the dataset into training and testing sets;

for$(training\ set)$

Perform the DSSGL to create the additional image samples;

Add these images to the training set;

Train EUNet to create the feature-level segmented maps and probability maps;

Get the final discriminative segmented feature map by fusing these 2 maps;

end for

for$(each\ discriminative\ segmented\ feature\ map)$

Train the fused DCNN classifier;

Test the fused DCNN classifier using the testing samples;

Validate the efficiency of classifying the ovarian carcinoma categories;

end for

End

4. Experimental results

In this section, the efficiency of DSSGL-EUNet-DCNN is analyzed by implementing it in Matlab 2017b with the help of the TCGA-OV dataset [25]. Among 497 CT scans, 350 scans (50 samples from every ovarian carcinoma category) are used for training and 147 scans (21 samples from every ovarian carcinoma category) are used for testing. Also, its efficiency regarding different metrics is compared with implementing the DSSGL-DCNN

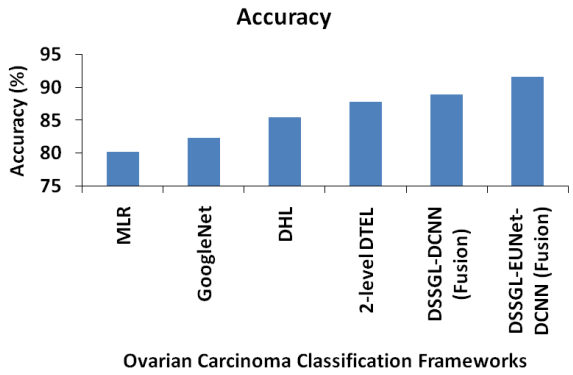

Figure. 6 Comparison of accuracy

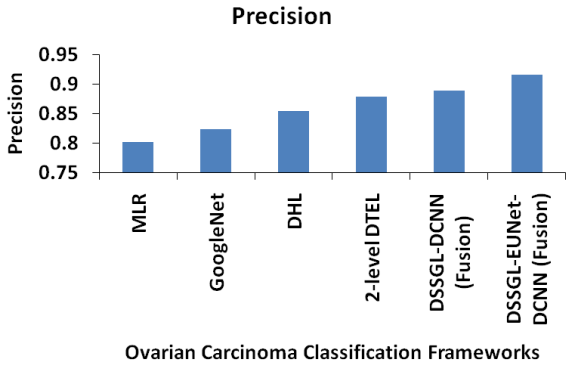

Figure. 7 Comparison of precision

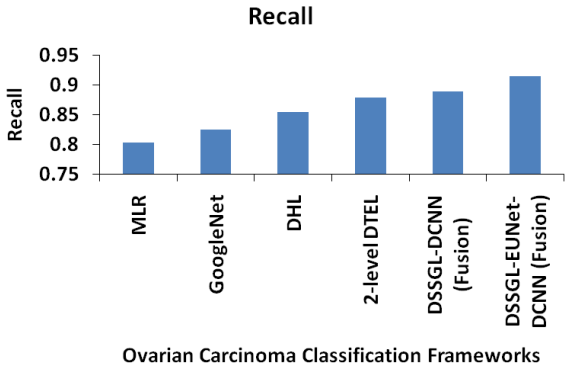

Figure. 8 Comparison of recall

(Fusion) [15], GoogleNet [19], 2-level DTEL [22], MLR [23], DHL [24] frameworks for ovarian carcinoma segmentation and classification.

4.1 Accuracy

It is the fraction of accurate classification of ovarian cancer categories over the total number of attempts executed.

$$Accuracy = \frac{TP+True\ Negative\ (TN)}{TP+TN+FP+FN} \quad (6)$$

TP is a result where the classifier categorizes ovarian cancers as themselves e.g., clear cell carcinoma is classified as clear cell carcinoma. TN is a result where the classifier categorizes the non-ovarian cancers as non-ovarian cancers. FP is a result where the classifier inexactly categorizes ovarian cancers as non-ovarian cancers. FN is a result where the classifier inexactly categorizes the non-ovarian cancers as ovarian cancers.

Fig. 6 displays the accuracy achieved for MLR, GoogleNet, DHL, 2-layer DTEL, DSSGL-DCNN (fusion), and DSSGL-EUNet-DCNN (fusion) frameworks to categorize the ovarian carcinomas. It examines that the DSSGL-EUNet-DCNN (fused structure) framework accomplishes a greater accuracy than the other frameworks i.e., the accuracy of DSSGL-EUNet-DCNN (fusion) is 14.19 % larger than the MLR, 11.21 % larger than the GoogleNet, 7.16 % larger than the DHL, 4.41 % larger than the 2-layer DTEL and 2.98 % larger than the DSSGL-DCNN (fusion) frameworks.

4.2 Precision

It is the ratio of exactly classified categories of ovarian cancers at true positive (TP) and false positive (FP) rates.

$$Precision = \frac{TP}{TP+FP} \quad (7)$$

Fig. 7 exhibits the precision obtained for MLR, GoogleNet, DHL, 2-layer DTEL, DSSGL-DCNN (fusion), and DSSGL-EUNet-DCNN (fusion) frameworks to categorize the ovarian carcinomas. It indicates that the DSSGL-EUNet-DCNN (fused structure) framework achieves a greater precision than the other frameworks i.e., the precision of DSSGL-EUNet-DCNN (fusion) is 14.17 % greater than the MLR, 11.22 % greater than the GoogleNet, 7.15 % greater than the DHL, 4.27 % greater than the 2-layer DTEL and 2.98 % greater than the DSSGL-DCNN (fusion) frameworks.

4.3 Recall

It is the ratio of exactly classified categories of ovarian cancers at TP and false negative (FN) rates.

$$Recall = \frac{TP}{TP+FN} \quad (8)$$

Fig. 8 shows the recall obtained for MLR, GoogleNet, DHL, 2-layer DTEL, DSSGL-DCNN (fusion), and DSSGL-EUNet-DCNN (fusion) frameworks to categorize the ovarian carcinomas. It indicates that the DSSGL-EUNet-DCNN (fused structure) framework achieves a greater recall than the other frameworks i.e., the recall of DSSGL-

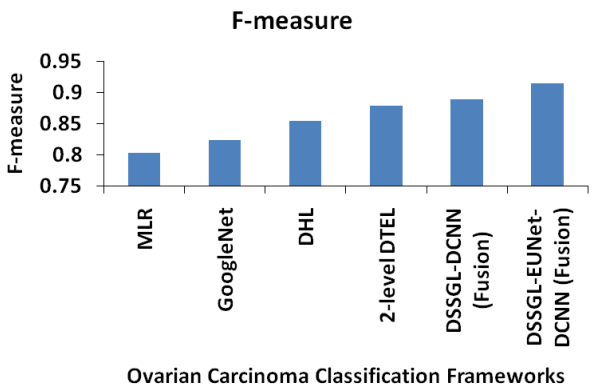

Figure. 9 Comparison of F-measure

EUNet-DCNN (fusion) is 13.99 % higher than the MLR, 11.04 % higher than the GoogleNet, 7.09 % higher than the DHL, 4.17 % higher than the 2-layer DTEL and 2.94 % higher than the DSSGL-DCNN (fusion) frameworks.

4.4 F-measure

It is computed as the harmonic average of precision and recall.

$$F - measure = 2 \times \frac{Precision \cdot Recall}{Precision + Recall} \quad (9)$$

Fig. 9 shows the f-measure obtained for MLR, GoogleNet, DHL, 2-layer DTEL, DSSGL-DCNN (fusion), and DSSGL-EUNet-DCNN (fusion) frameworks to categorize the ovarian carcinomas. It indicates that the DSSGL-EUNet-DCNN (fused structure) framework achieves a greater recall than the other frameworks i.e., the recall of DSSGL-EUNet-DCNN (fusion) is 14.07 % higher than the MLR, 11.12 % higher than the GoogleNet, 7.11 % higher than the DHL, 4.19 % higher than the 2-layer DTEL and 2.92 % higher than the DSSGL-DCNN (fusion) frameworks.

5. Conclusion

In this article, a DSSGL-EUNet-DCNN framework is designed to improve the accuracy of classifying ovarian carcinoma. At first, the training CT scans are augmented by the DSSGL and fed to the EUNet. This EUNet comprises different units: the IR unit, the DI unit, the downsampling and the upsampling units to create the feature-level segmented maps for a given CT scan. Also, the feature-level probability map is generated and thresholded to binary. This map is further merged with the feature-level segmented maps to create the discriminative segmented sample. This resultant segmented sample is fed to the fused structure-based DCNN to train and classify the types of ovarian carcinomas. To conclude, the findings revealed that the DSSGL-EUNet-DCNN seems to have an accuracy of 91.63 % compared to the MLR, GoogleNet, DHL, 2-level DTEL and DSSGL-DCNN frameworks for segmenting and categorizing ovarian cancer types. However, the efficiency of this classification depends on the selection of DCNN hyperparameters. So, the future work will focus on optimizing the hyperparameters used for DCNN training to enhance the accuracy.

Conflict of interest

The authors declare no conflict of interest.

Author contributions

Conceptualization, methodology, software, validation, Pillai Honey; formal analysis, investigation, Tajunisha; resources,data curation, writing—original draft preparation, Pillai Honey; writing—review and editing, Pillai Honey; visualization,; supervision, Tajunisha;

References

[1] S. Hauptmann, K. Friedrich, R. Redline, and S. Avril, “Ovarian borderline tumors in the 2014 WHO classification: evolving concepts and diagnostic criteria”, *Virchows Archiv*, Vol. 470, No. 2, pp. 125-142, 2017.

[2] V. W. Chen, B. Ruiz, J. L. Killeen, T. R. Coté, X. C. Wu, C. N. Correa, and H. L. Howe, “Pathology and classification of ovarian tumors”, *Cancer: Interdisciplinary International Journal of the American Cancer Society*, Vol. 97, No. S10, pp. 2631-2642, 2003.

[3] M. B. Daly, R. Pilarski, M. B. Yurgelun, M. P. Berry, S. S. Buys, P. Dickson, and S. D. Darlow, “NCCN guidelines insights: genetic/familial high-risk assessment: breast, ovarian, and pancreatic, version 1.2020: featured updates to the NCCN guidelines”, *Journal of the National Comprehensive Cancer Network*, Vol. 18, No. 4, pp. 380-391, 2020.

[4] W. Chan, M. Lee, Z. X. Yeo, D. Ying, K. A. Grimaldi, C. Pickering, ... and L. C. Tzang, “Development and validation of next generation sequencing based 35-gene hereditary cancer panel”, *Hereditary Cancer in Clinical Practice*, Vol. 18, No. 1, pp. 1-8, 2020.

[5] A. D. Leo, D. Santini, C. Ceccarelli, G. Santandrea, A. Palicelli, G. Acquaviva, ... and D. D. Biase, “What is new on ovarian carcinoma: integrated morphologic and

molecular analysis following the new 2020 world health organization classification of female genital tumors", *Diagnostic*s, Vol. 11, No. 4, pp. 1-16, 2021.

[6] L. Castéra, S. Krieger, A. Rousselin, A. Legros, J. J. Baumann, O. Bruet, and D. Vaur, "Next-generation sequencing for the diagnosis of hereditary breast and ovarian cancer using genomic capture targeting multiple candidate genes", *European Journal of Human Genetics*, Vol. 22, No. 11, pp. 1305-1313, 2014.

[7] R. M. Dewi and U. N. Wisesty, "Classification of polycystic ovary based on ultrasound images using competitive neural network", *Journal of Physics: Conf. Series*, Vol. 971, No. 1, pp. 1-8, 2018.

[8] J. Nuhić, L. Spahić, S. Ćordić, and J. Kevrić, "Comparative study on different classification techniques for ovarian cancer detection", In: *Proc. of International Conf. on Medical and Biological Engineering*, Springer, Cham, pp. 511-518, 2020.

[9] H. Lalremmawia and B. K. Tiwary, "Identification of molecular biomarkers for ovarian cancer using computational approaches", *Carcinogenesis*, Vol. 40, No. 6, pp. 742-748, 2019.

[10] S. Nougaret, M. Tardieu, H. A. Vargas, C. Reinhold, S. V. Perre, N. Bonanno, and I. T. Naggara, "Ovarian cancer: an update on imaging in the era of radiomics", *Diagnostic and Interventional Imaging*, Vol. 100, No. 10, pp. 647-655, 2019.

[11] C. Wu, Y. Wang, and F. Wang, "Deep learning for ovarian tumor classification with ultrasound images", In: *Proc. of Pacific Rim Conf. on Multimedia*, pp. 395-406, 2018.

[12] A. Kleppe, O. J. Skrede, S. D. Raedt, K. Liestøl, D. J. Kerr, and H. E. Danielsen, "Designing deep learning studies in cancer diagnostics", *Nature Reviews Cancer*, pp. 119-211, 2021.

[13] T. G. Debelee, S. R. Kebede, F. Schwenker, and Z. M. Shewarega, "Deep learning in selected cancers' image analysis – a survey", *Journal of Imaging*, Vol. 6, No. 11, pp. 121, 2020.

[14] P. Mathialagan and M. Chidambaranathan, "Analysis and classification of H&E-stained oral cavity tumour gradings using convolution neural network", *International Journal of Intelligent Engineering & Systems*, Vol. 14, No. 5, pp. 517-528, 2021, doi: 10.22266/ijies2021.1031.45.

[15] N. P. Honey and N. Tajunisha, "Automatic classification of ovarian cancer types from CT images using deep semi-supervised generative learning and convolutional neural network", *Revue D'intelligence Artificielle* ,Vol. 35, No. 4, pp. 273-280, 2021.

[16] O. Ronneberger, P. Fischer, and T. Brox, "U-net: Convolutional networks for biomedical image segmentation", In: *Proc. of International Conf. on Medical Image Computing and Computer-Assisted Intervention*, Springer, Cham, pp. 234-241, 2015.

[17] O. Klein, F. Kanter, H. Kulbe, P. Jank, C. Denkert, G. Nebrich, ... and E. T. Taube, "MALDI-imaging for classification of epithelial ovarian cancer histotypes from a tissue microarray using machine learning methods", *Proteomics - Clinical Applications*, Vol. 13, No. 1, pp. 1-26, 2018.

[18] E. Amidi, A. Mostafa, S. Nandy, G. Yang, W. Middleton, C. Siegel, and Q. Zhu, "Classification of human ovarian cancer using functional, spectral, and imaging features obtained from in vivo photoacoustic imaging", *Biomedical Optics Express*, Vol. 10, No. 5, pp. 2303-2317, 2019.

[19] K. H. Yu, V. Hu, F. Wang, U. A. Matulonis, G. L. Mutter, J. A. Golden, and I. S. Kohane, "Deciphering serous ovarian carcinoma histopathology and platinum response by convolutional neural networks", *BMC Medicine*, Vol. 18, No. 1, pp. 1-14, 2020.

[20] H. Yaghoobi, E. Babaei, B. M. Hussen, and A. Emami, "EBST: an evolutionary multi-objective optimization based tool for discovering potential biomarkers in ovarian cancer", *IEEE/ACM Transactions on Computational Biology and Bioinformatics*, pp. 1-11, 2020.

[21] S. K. Prabhakar and S. W. Lee, "An integrated approach for ovarian cancer classification with the application of stochastic optimization", *IEEE Access*, Vol. 8, pp. 127866-127882, 2020.

[22] Y. Wang, D. Farnell, H. Farahani, M. Nursey, B. T. Cloutier, S. J. Jones, ... and A. Bashashati, "Classification of epithelial ovarian carcinoma whole-slide pathology images using deep transfer learning", *arXiv Preprint arXiv:2005.10957*, 2020.

[23] S. Li, J. Liu, Y. Xiong, P. Pang, P. Lei, H. Zou, ... and P. Luo, "A radiomics approach for automated diagnosis of ovarian neoplasm malignancy in computed tomography", *Scientific Reports*, Vol. 11, No. 1, pp. 1-9, 2021.

[24] D. Sengupta, S. N. Ali, A. Bhattacharya, J. Mustafi, A. Mukhopadhyay, and K. Sengupta, "A deep hybrid learning pipeline for accurate

diagnosis of ovarian cancer based on nuclear morphology", *PloS One*, Vol. 17, No. 1, pp. 1-20, 2022.
[25] https://wiki.cancerimagingarchive.net/display/Public/TCGA-OV